1-1-2014

Influence of Back Electrostatic Field on the Collection Efficiency of an Electrostatic Lunar Dust Collector

Nima Afshar-Mohajer

Yatit Thakker

Chang-Yu Wu

Nicoleta Sorloaica-Hickman
University of Central Florida

Aerosol and Air Quality Research, 14: 1333–1343, 2014

ISSN: 1680-8584 print / 2071-1409 online
doi: 10.4209/aaqr.2013.12.0353

Influence of Back Electrostatic Field on the Collection Efficiency of an Electrostatic Lunar Dust Collector

Nima Afshar-Mohajer[1], Yatit Thakker[1], Chang-Yu Wu[1*], Nicoleta Sorloaica-Hickman[2]

[1] *Department of Environmental Engineering Sciences, Engineering School of Sustainable Infrastructure and Environment, University of Florida, Gainesville, FL 32611, USA*
[2] *Florida Solar Energy Center, University of Central Florida, Cocoa, FL 32922, USA*

ABSTRACT

Protecting sensitive surfaces from dust deposition in the limiting condition of the lunar atmosphere is imperative for space exploration. In this study, how back electrostatic field due to charge build-up on collection plates may affect the performance of an electrostatic lunar dust collector (ELDC) was investigated. The relationships between ELDC dimensions, collection efficiency and electrical properties of lunar dust particles were derived to develop a model, appropriate for any size of the ELDC. A Lagrangian-based discrete element method (DEM) was applied to track particle trajectories, and sensitivity analyses were conducted for the concentration of the incoming particles, the number of pre-collected particles and the applied voltages. The results revealed that the collection efficiency reduced over time due to the back electrostatic field of the collected particles, which ultimately led to a suspended regime, rather than just collected and penetrated fractions considered in conventional models. The generated back electrostatic field and the cloud of suspended particles were strong enough to disrupt the performances of both the ELDC and the protected device. The maximum time ELDC can run without significant loss in collection efficiency was estimated to be 10 terrestrial days for the studied ELDC size and applied voltage. Because the electrical power was negligible compared to the provided power by the solar panels, increasing the applied voltage was found to be the best option to counteract back electrostatic growth.

Keywords: Lunar dust; Back electrostatic field; Collection efficiency; Discrete element method.

INTRODUCTION

Dusty environment of the lunar surface was troublesome in previous NASA explorations. A cloud of levitated lunar grains with high affinity of adhering to the nearby surfaces, which hampered the lunar surface operations, was observed during the entire Apollo program (from 1969 to 1973) (Gaier, 2005; Stubbs *et al.*, 2006; Colwell *et al.*, 2009; Gaier *et al.*, 2011). Due to the rarefied atmosphere of the moon and absence of a strong magnetic field, the lunar surface is not shielded from high energetic solar radiation and solar winds (Abbas *et al.*, 2007; Colwell *et al.*, 2009; Calle *et al.*, 2011). While photoemissive radiation (e.g., UV and X-ray) on lunar dayside accumulate positive charges, impingement of electrons on lunar nightside leads to negative charge accumulation on lunar grains (Walch *et al.*, 1995; Halekas *et al.*, 2002; Halekas *et al.*, 2008; Dove *et al.*, 2010). The like-charged particles create a local electric field near the surface, which lifts the particles off from the lunar surface because of interparticle repelling forces (Stubbs *et al.*, 2006; Colwell *et al.*, 2009). The majority of the levitated adhesive particles fall back toward the lunar surface (See Fig. 1) and deposit on the exposed equipment surfaces, causing obscuration of solar panels (Mazumder *et al.*, 2003), dimness of optical surfaces, degradation of thermal surface performance (Gaier *et al.*, 2011), false measurements by instruments and frequent replacement of costly devices. Therefore, starting from early 90's, the National Aeronautics and Space Administration (NASA) has established dust mitigation programs to study all the possible lunar and Martian dust control technologies for future exploratory space missions.

Considering the limiting conditions of the lunar environment, an electrostatic lunar dust collector (ELDC) was proposed to protect exposed surfaces from the falling lunar particles. The ELDC configuration and the way it operates have been described in previous studies in detail (Afshar-Mohajer *et al.*, 2011, 2012). In summary, an ELDC consists of a grid layer of parallel transparent plates normal to the surface to be protected. Each pair of conducting ELDC plates are connected to the positive and negative terminals of the DC power supplied by the solar panels.

* Corresponding author.
Tel.: 1-352-392-0845; Fax: 1-352-392-3076
E-mail address: cywu@ufl.edu

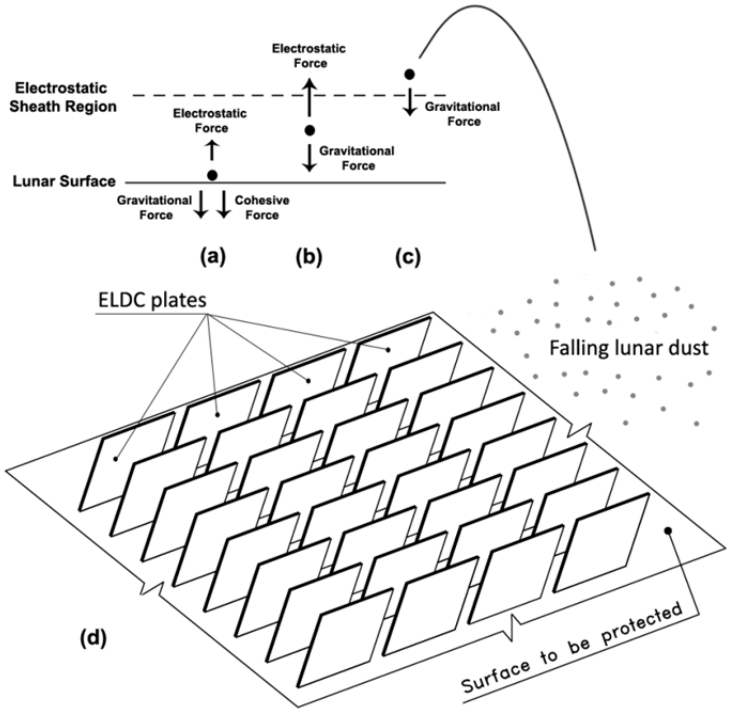

Fig. 1. Free body diagrams for a near-surface fine lunar grain a) on the lunar surface, b) levitated inside the electrostatic sheath region, c) falling down outside the electrostatic sheath region; and d) Schematic of the ELDC plates arrangement to protect installed surfaces

Since vacuum filling the space between the plates is an insulator, the ELDC acts as an electrical capacitor. The generated electrostatic field enables the ELDC plates to collect the naturally charged falling lunar particles possessing the opposite electric polarity (see Fig. 1(d)). Due to the transparency of the ELDC plates and the fact that solar panels are programmed to orientate normally to the sun, deterioration in panel performance due to blockage of sun light by ELDC plates should not be a concern.

Adequacy of ELDC application in lunar dust collection was previously demonstrated using both analytical and numerical models. The simulations on 20-μm particles concluded that applying a 3.5 kV/m electric field is sufficient for 100% collection efficiency at the most conservative scenario (Afshar-Mohajer *et al.*, 2011, 2012). The main advantage of the ELDC over other electrical methods is its low power requirement in lunar dust collection. For instance, the electrodynamic shield (EDS) consisting of embedded electrodes connected to an AC power supply inside an insulating film has been proven to be an effective lunar dust mitigation method. However, Qian *et al.* (2011) pointed out that the power required for proper electric curtain operation of the EDS can be higher than the power generated by the solar panels; thus, an optimal on-and-off control procedure is needed to ensure feasibility of the EDS. The electrostatic lunar dust repeller (ELDR) is another electrical method that brings some advantages of no need of cleaning and light weightiness. Nonetheless, it operates at about 10 times higher voltages compared to the ELDC, and it is only suitable for surfaces smaller than 30 cm^2 (Afshar-Mohajer *et al.*, 2014).

In spite of high efficiency of the ELDC in particle collection, its collection plates attract incoming particles continuously and as time goes by, a layer of deposited particles carrying the opposite charge builds up on the plate. Collected fine particles stay on the plates due to strong surface forces as well as electrostatic attraction between the particles and the collection plate. The process of particle deposition on the collection plates forms a back electrostatic field which strengthens with time (Zukeran *et al.*, 1999), and influences proper collection of the later approaching particles. The effect of such an undesirably formed electrostatic field was not considered in all the previous studies regarding lunar dust collection. Since cleaning the ELDC plates in the lunar environment with constraining resources is inconvenient, this study was aimed to investigate the significance of the back e-field as a function of time and to optimize the ELDC operation accordingly.

Although the proposed ELDC has similarities to terrestrial electrostatic precipitators (ESPs), the main difference arises from the fact that no drag forces are acting on the particles to decelerate particles inside the hard vacuum. As a result, the classic equations derived for the conventional ESPs are not valid for the ELDC. Although back corona and particle re-entrainment are the most common problems in ESP operation, injecting adhesive agents, performing wet ESP and frequent rapping of collecting electrodes provide a wide range of solutions for retaining the collection efficiency for terrestrial applications (Mizuno, 2000). However, all of the mentioned methods are impractical and inconvenient in lunar environment, the limitation of which warrants the need for obtaining insights into the frequency of ELDC plate cleaning.

METHODS

Obtaining the ELDC collection efficiency at any point of time requires Lagrangian-based modeling to track particle trajectories individually. First, representative lunar particle characteristics were decided using previously developed models. Then, ELDC dimensions were determined and Poisson's equation was solved numerically to obtain charge distribution on the ELDC plates. Considering the acting forces on each particle, the trajectory of all the lunar particles were tracked and recorded at each time step by later discussed Lagrangian-based model. The fate of any individual particle was determined by analyzing the output logs. Finally, sensitivity analyses were conducted on the concentration of the incoming particles, the number of particles collected before introduction of the incoming particles and the applied voltage (electrostatic field strength).

Lunar Dust Particles

Exposure of lunar grains to hypervelocity meteorite impacts leads to a wide particle size range and shape irregularity (jagged edges with mean aspect ratio of about 0.7) (Liu *et al.*, 2008). In this study, we follow the definition of lunar dust by Park *et al.* (2008) for lunar particles smaller than 20 μm (50 to 80% by weight). Lunar dust consists of materials almost entirely from impact glass along with nano-phase iron. According to Walton (2007), its density (ρ_p) ranges from 2.3 to 3.2 g/cm^3 with a recommended value of 3.1 g/cm^3 for general scientific studies.

The ultimate fate of levitated lunar dust depends on particle size, particle surface charge and particle-particle interactions. The ultra-vacuum condition of the lunar atmosphere makes all particles accelerate toward the lunar surface in the absence of resistive forces. This condition also helps particles to better maintain their accumulated surface charges (Schmitt *et al.*, 1991). Since gravitational force is proportional to particle volume (d_p^3), electrostatic collection of lunar particles becomes harder with an increase in particle size (Afshar-Mohajer *et al.*, 2011). On the other hand, Stubbs *et al.* (2006) has demonstrated that the maximum height for the levitated particles is inversely proportional to d_p^2. Considering these opposing effects of particle size for the most conservative case (i.e., most difficult scenario for lunar dust collection), the largest particle size in which significant particle levitation occurs was chosen based on the surface potential of the lunar dust, which affects particle levitation height.

The surface potential of the lunar particles has been investigated through both in-situ measurements and theoretical models. However, since surface potential is sensitive to the lunar Debye length and solar plasma flow conditions over the lunar grains, reported values for the surface potential from different studies differ greatly. For instance, Manka (1973) and Farrell *et al.* (2007) used a plasma model at the terminator suggesting 50 V for the lunar surface potential while the particle-in-cell simulations of Wang *et al.* (2008) on Poisson's equation resulted in the surface potential ranging from 0 to ±30 V. On the other hand, measurements by lunar prospector obtained the range of –35 to –100 V on the lunar night side (Dove *et al.*, 2010). Since particles accumulate charges on their surfaces, the upper limit of the reported values was opted for this study. Goertz (1989) has offered a simple model for estimating accumulated surface charge on lunar particles as follows:

$$q_p = 2\pi\varepsilon_0 d_p \phi_s \tag{1}$$

where ε_0 is the vacuum permittivity (8.854×10^{-12} F/m), d_p is particle diameter and ϕ_s is lunar surface potential. The dynamic fountain model presented by Stubbs *et al.* (2006) was then used to obtain the corresponding particle size knowing surface potential and particle density as in Eq. (2):

$$d_p = \sqrt{\frac{12\varepsilon_0 \phi_s^{\,2}}{\rho_p g_l Z_{max}}} \tag{2}$$

where Z_{max} is the maximum levitation height of the lunar dust, g_l is lunar gravitational acceleration (1.62 m/s^2). In this model, once lunar dust attains sufficient charge to overcome gravitational force and cohesive forces, it levitates from the lunar surface and accelerates upward. When particles leave the sheath region outside of which only lunar gravity acts on the particles, they follow a near parabolic trajectory and fall back toward the lunar surface from their maximum levitation height (Stubbs *et al.*, 2006) (see Fig. 1(a)–1(c)). Considering the free-fall motion of the falling particles from the maximum levitation height inside the vacuum, the initial velocity of the particles at the ELDC entrance are equal to the exit velocity of the particles leaving the sheath region. Thereby, Eq. (3) relates the initial velocity of the lunar particles to the other properties (Afshar-Mohajer *et al.*, 2011):

$$v_{0p} = \frac{2\phi_s}{d_p}\sqrt{\frac{6\varepsilon_0}{\rho_p}} \tag{3}$$

All the representative values were opted appropriately to evaluate ELDC proficiency in the most conservative cases. Positively charged lunar particles were considered on dayside at the upper limit of the reported ranges for particle density and surface potential (ρ_p = 3.1 g/cm^3 and ϕ_s = 100 V). Assuming 0.5 m as the lowest levitation height at which lunar particles threat an exposed solar panel, Eq. (2) gives the corresponding particle size as $d_p \cong 20$ μm. In other words, lunar grains larger than 20 μm possess a levitation height too low (less than 50 cm) to be a threat for the exposed surfaces. On the other hand, while the levitation height of the lunar particles smaller than 20 μm is higher, their electrostatic collection is easier for the ELDC design (Afshar-Mohajer *et al.*, 2011). Thus, 20 μm spherical particles with the density, surface charge, initial velocity at the ELDC entrance and mechanical properties defined above were opted for simplicity of the numerical computations.

ELDC Configuration

Fig. 2 shows a pair of square and parallel plates which

represent the ELDC within the provided model. The dimensional ratio of L/D = 2 was maintained throughout the simulations, where D is the spacing between the plates and L is the plate height. Since the relationship between the collection efficiency and L/D ratio has been discussed in prior studies, all later obtained results can be easily transformed for another L/D ratio using the derived analytical equation (Afshar-Mohajer *et al.*, 2011).

The most conservative case in which ELDC shows the lowest collection efficiency was considered, i.e., ELDC plates were aligned normally to the lunar surface (in y-z plane) and all falling particles were subjected to the lunar gravity in the z-direction. Two separate sets of particles were created initially inside two different box-shaped domains, so-called Particle Factories 1 and 2, before the start of each simulation (see Fig. 2(a)). Particle Factory 1 created "pre-collected" particles carrying positive charges on the ELDC plates before simulation runs. Although fringe effect more favorably attracts particles closer to the edges of the collection plate, model limitation requires that Particle Factory 1 placed particles uniformly on the ELDC plates. The same numbers of particles were assumed in columns and rows to cover the entire D × W area of the ELDC entrance as shown in Fig. 2(b). Pre-collection of charged particles on the collection plate requires an assumption of a thin insulation film between the collection plate and Particle Factory as will be discussed later. The role of Particle Factory 2 was to create falling particles. Concentration of the incoming particles and loading of the pre-collected particles were addressed by taking different values for the number of rows and columns (m and n) within particle factories (see Fig. 2(b)).

The concentration of levitated lunar particles is not well documented. According to measured data by Surveyor-7 Lander, it has been approximated as 50 particles/cm^3 (Criswell, 1973). The needed run time to detect particle interactions in DEM simulation for a system made of n particles is proportional to n^2. So, a smaller ELDC helps running simulations for the measured range of lunar dust concentration in a reasonable time scale. Providing an appropriate model to be applicable for any ELDC configuration is imperative, and requires finding reasonable relationships between all ELDC key parameters including ELDC dimensions, applied voltage, surface charges and collection efficiency. To do so, a new approach was taken using well known concepts of ELDC capacitance and acting forces on lunar particles in this study.

The ELDC capacitance, C, is defined as the ratio of the total charge on each plate, Q, over the provided electrical

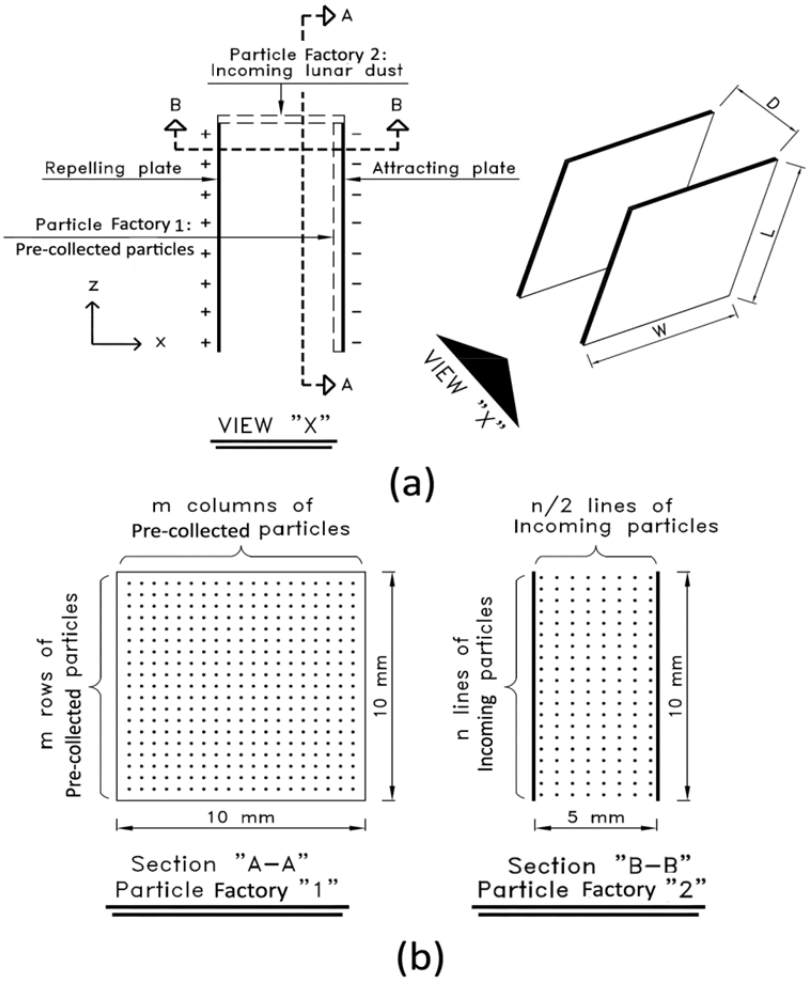

Fig. 2. a) A section of the ELDC on the x-z plane b) Lunar particles arrangement in the DEM model at t = 0.

potential between the conducting parallel plates, ΔV. On the other hand, since ELDC capacitance is a function of ELDC dimensions (L, W, D) and the type of the insulating medium, ε_0, it serves as a measure for ELDC scaling:

$$C = \frac{Q}{\Delta V} = \varepsilon_0 \frac{L \times W}{D} \tag{4}$$

There are three major forces that act on falling lunar particles: gravitational force, electrostatic force due to the charges on ELDC plates, and interparticle electrostatic forces; dielectrophoresis is neglected, and there are no resistive forces in the lunar atmosphere. Independent from ELDC sizing, the gravitational force, F_G, is a constant but the electrostatic force, F_E, is governed by Coulomb force as the following (Hinds, 1982):

$$F_E = q_p E = q_p \frac{q' K_E}{R^2} \tag{5}$$

where K_E is the electrical constant (9×10^9 Nm^2/C^2), q' is either a point charge on the ELDC plates or the charge of another lunar particle and R is the magnitude of the position vector connecting the assumed particle to the other point charge or charged particle. Resizing the ELDC dimensions α times smaller changes interparticle distances and the distances between particles and point charges on the collection plate α times smaller. This reduces R value in Eq. (5) α times, leading to α^2 times increase in the pertinent electrostatic force. To obtain the same collection efficiency from ELDCs with different sizes, all acting forces on particles with certain properties must be unchanged. Eq. (5) concludes the way to maintain the same values for electrostatic forces of α times smaller ELDC, is to multiply both q_p and q' by a correction factor of (1/α). Then, Eq. (4) obtains the corresponding applied voltage for the new ELDC dimensions with the corrected total surface charges. Since particles and point charges on ELDC plates all behave as charged points in DEM modeling, higher concentration of the falling lunar particles and loading on the collection plate with corrected charge values for the rescaled ELDC produce the same electrical effects and collection efficiencies. Table 1 summarizes how ELDC resizing and its correction factor affect other key parameters of the DEM model.

As we have explained in our prior studies, the ideal ELDC dimensions are L = W = 10 cm and D = 5 cm. However, in order to handle the reported value of lunar dust number concentration and expedite the DEM simulations run time in this study, the ELDC dimensions were selected as L = W = 10 mm and D = 5 mm which are 10 times smaller than the values used in the prior studies. Using the aforementioned correction method, our modeling results can be considered for the real size ELDC (L = W = 10 cm and D = 5 cm), since the total surface charge on the ELDC plates (Q) and particle charge (q_p) were modified with the correction factor 0.1 to cancel out ELDC resizing effect inside the DEM model.

Non-uniform Electrostatic Field

The ratio of L/D = 2 adopted in this study results in denser charge accumulation at the edges (fringe effect) (Ulaby, 2010). So, the suggested model from basic electrostatics assuming uniformity of the generated e-field and charge distribution on the conducting plates is not valid (Nishiyama and Nakamura, 1994; Catalan-Izquierdo *et al.*, 2009). We used the method extracted from a previous study (Reitan and Higgins, 1951; Reitan, 1959) to accurately find the charge distribution on the ELDC plates. In short, each plate was discretized into a number of identical subplates with uniformly distributed charges within each subplate. Providing a stable potential difference between the ELDC plates, the electrical potentials on all of the subplates from the same ELDC plate are equal to $\Delta V_i = \pm \Delta V/2$ (ΔV is the provided electrical potential between the ELDC plates). Then, Eq. (6) which is the integral form of the Poisson's equation was solved numerically using MATLAB 7.10 codes to obtain the surface charge density over each subplate:

$$\Delta V_i = \int_s \frac{\rho_s ds}{4\pi\varepsilon_0 \vec{R}} \tag{6}$$

where ΔV_i (electrical potential of i^{th} subplate) is equal to $+\Delta V/2$ for i = 1, 2,…, k on the positively charged plate, and ΔV_i is equal to $-\Delta V/2$ for i = k + 1, k + 2,…, 2k on the negatively charged plate. $\vec{R}$ is the position vector between any two points on the ELDC plates, ρ_s is the surface charge density and s refers to the area of each plate. The capacitance of the ELDC was used as a measure to determine the appropriate number of subplates.

For a conducting collection plate, the above mentioned procedure only obtains the initial charge distribution on the plates in that the collected charges will be redistributed on the surface of the conducting plate after the attraction of any approaching particle. This means the collected particle reduces the total surface charge on the plate as it possesses the opposite charge. Since there was only small reduction in the total surface charge of the collection plate (0.3% reduction per collected particle in this study) and consequently the updating charge distribution was not critical, the calculated non-uniform electrostatic field was maintained throughout the simulation. This justifies the assumption of considering a thin layer of insulation in front of the collection plate to prevent charge redistribution on its surface.

Table 1. Correction factors of key parameters after ELDC resizing

Resizing factor of the ELDC dimensions	Particle charge (q_p)	Total charge on collection plate (Q)	ELDC capacitance (C)	Electrical potential between ELDC plates (ΔV)
α	1/α	1/α	α	1

Discrete Element Method

Application of continuum based methods such as finite element to study the dynamics of charged particles in tenuous atmosphere of lunar environment are plagued by the need for incorporating mechanical contacts and electrical interactions of falling particles. The discrete element method (DEM) originally developed by Cundall and Strack (1979) has proven to be a powerful numerical tool to include interparticle forces by tracking individual particles at each time step (Liu *et al.*, 2010).

DEM is a computational intensive algorithm starting with initial placement of the particles. In this study, acting forces on each particle including gravitational force, external electrostatic force, interparticle electrical forces and mechanical contacts, were considered. The particle acceleration vector was calculated according to Newton's second law. Particles were repositioned for the next time step based on the kinematic equations of motion. The same procedure repeated for the entire run time. EDEM 2.4.2 developed by DEM Solutions Inc., which has incorporated electrostatic calculations with flexibilities in designing different geometries and simulation set up, was applied for this study.

The DEM model detects both particle collisions and electrical particle-particle interactions. Hertz-Mindlin equation with no particle slip, which is a soft contact force model based on frictional elasticity of a spherical particle in contact with wall or other particles, which is known as the preferred model for low impact particulate systems (Di Renzo and Di Maio, 2004), was used for the particle collisions. Since a Cartesian grid discretizes the ELDC geometry into 3D cells, detecting particle collisions for each particle is limited to the cell confining the target particle and the adjacent grid cells. DEM discretization promises to provide a better numerical convergence with refinement of the grid cells (Tavarez and Plesha, 2007). Sensitivity analysis on grid cell size demonstrated that grid sizes finer than 0.2 mm do not influence the obtained particle trajectories. Hence, 0.2 mm was opted as the grid cell size in this study. As for electrical particle-particle interactions, the electrical screening distance, λ, was defined as the radius of an imaginary sphere around each centered particle. Thus, only particles located inside the formed sphere of influence would be involved in calculating the interparticle electrical forces on the centered particle. Studying re-entrainments and back e-field requires inclusion of all the particles in interparticle electrical calculations. Therefore, λ = 5 mm was taken as the radius of the electrical screening sphere to cover the entire ELDC geometry and to ensure all distributed point charges on the ELDC plates, pre-collected particles and falling incoming lunar particles have been included in calculating the acting forces on any target particle.

When ELDC starts working, all particles are attracted toward the collection plate. As such, particles travel a longer distance to exit compared to the case with no applied e-field. The total time, T, in which a 20-μm-sized lunar particle passes through an unpowered ELDC, is easy to calculate as it is just the elapsed time for the vertical free fall of the particle under lunar gravity with an initial velocity obtained from Eq. (3). Double of such needed time was considered as the total run time.

The time step in DEM modeling is a function of particle stiffness and mass of the smallest particle (Tavarez and Plesha, 2007). Depending on particle concentration, 20% to 40% of the Rayleigh time step has been suggested as the suitable time step for EDEM program. The Rayleigh time step, t_R, is the time taken for a shear wave to propagate through a solid particle and it is defined as:

$$t_R = \frac{\pi d_p}{(0.3262\upsilon_p + 1.7532)}\sqrt{\frac{\rho_p}{G_p}} \tag{7}$$

where G_p and υ_p are shear modulus and Poisson's ratio of the lunar particles. Thereby 20% of the Rayleigh time step with properties of JSC-1a lunar dust simulants ($G_p = 2.66 \times 10^7$ Pa and υ_p = 0.43 from Alshibli and Hasan, 2009) gave 3.6×10^{-7} s as the simulation time step.

A Dell Precision T5500 Workstation with 8 Intel(R) Xenon(R) CPU E5620 cores, processing speed of 2.4 GHz, and 8 GB DDR3 as RAM was dedicated to run the DEM simulations. Apparently, the simulation run time is a function of the total number of particles, electrical screening distance, cell grid size and time step. The longest simulation run time, which was about 1.5 hr, belonged to the case including 64 incoming particles and 900 pre-collected particles.

Analysis of Particle Trajectories

The DEM model records positions of all the particles at each time step. Investigating the fate of the particles requires analysis of the obtained trajectories to determine if a particle is collected. The DEM model produces separate output logs for each direction (x, y or z); Visual Basic for Applications (Microsoft VBA 7.0) code was developed to identify particles and to sort each particle coordinate as (x, y, z). Then, MATLAB 7.10.0 code displayed the 3D graph of the particle trajectories to provide insight into defining 3 possible cases for the particles at the end of the simulation: collected, penetrated and suspended. Finally, another set of VBA code was developed to classify all the particles and to calculate the fraction within each class. A number of assumptions were made for particle classification as below:

- If a particle reaches the collection plate before leaving the ELDC within the simulation run time, it is considered as collected.
- If a particle leaves ELDC before reaching the collection plate within the simulation run time, it is considered as penetrated.
- Particles may be repelled back after reaching the collection plate due to the back e-field created by the pre-collected particles.
- Suspended particles are simply the fraction of particles which have neither been collected nor penetrated within the simulation run time. A fraction of particles leaves the ELDC through the y-direction before passing the entire length of L in the z-direction. This is also classified as suspended.

- Pre-collected particles (generated by Particle Factory 1) do not move throughout the simulation.

RESULTS AND DISCUSSION

Effect of Non-uniform Electrostatic Field

The non-uniform distributions of the obtained surface charge on the collection plates were determined at two applied voltages of 50 V and 100 V on each ELDC subplate by solving Eq. (6) numerically. Using the provided MATLAB code for this particular ELDC geometry, the ELDC capacitance was plotted as a function of the number of ELDC subplates as shown in Fig. 3. Although the total capacitance increased with an increase in the number of ELDC subplates, the rate of increase decreased as a result of the asymptotic trend. Since for any number of subplates greater than 100, changes in the ELDC capacitance was less than 2%, each ELDC plate was divided into 100 subplates.

Qualitative Observation of Particle Trajectories

The graphical feature of EDEM 2.4.2 provides a real-time observatory tool to track particle trajectories. For the same number of falling particles, the cross-sectional snapshots in the x-z plane were taken to observe the effect of the back electrostatic field at certain elapsed time of the simulation. Similar to re-entrainment and back flow in conventional ESPs (Miller *et al.*, 1998), the provided images illustrated how particles approaching the collection plate changed direction and got repelled back from the plate due to back e-field (see Fig. 4). This effect is clearly strengthened at higher loadings of the pre-collected particles with the same concentrations of the incoming particles. However, at the same loading of the pre-collected particles and point of time, an increase in particle concentration led to irregular suspension patterns instead of the observed circulation regions. The reason is that falling particles are mobile in contrast to the pre-collected particles. Thus, increasing the

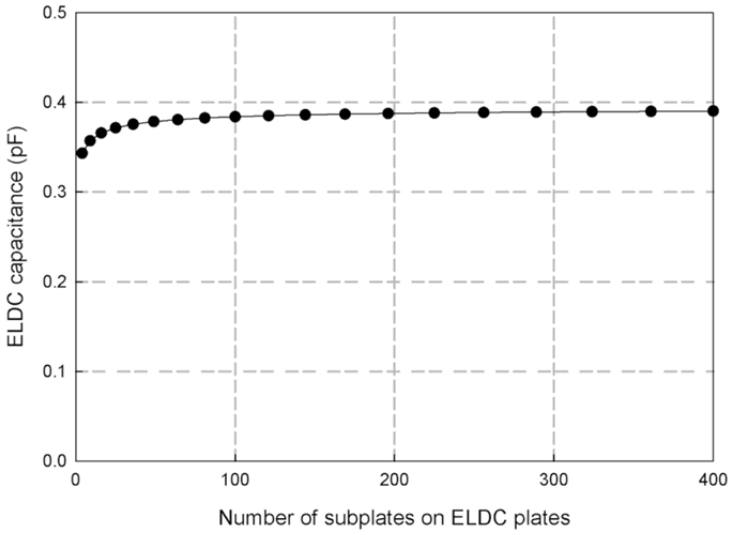

Fig. 3. ELDC capacitance as a function of the number of subplates.

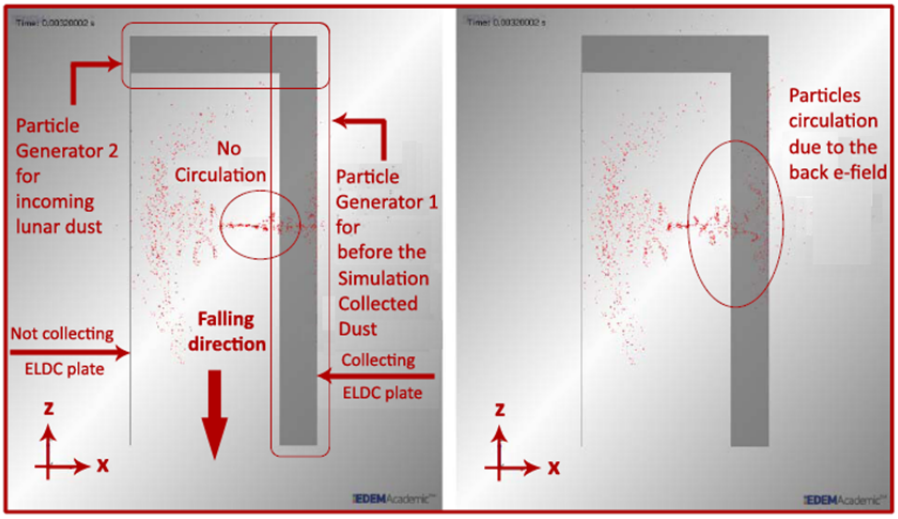

Fig. 4. Trajectories of the falling lunar dust in absence (left) and presence (right) of pre-collected particles, at otherwise the identical simulation conditions.

number of moving particles results in more chaos in the observed suspension pattern. Fig. 4 presents the mentioned particle circulation regions in the vicinity of the collection plate at an intentionally high concentration of the incoming particles (3200 #/cm^3).

Effect of Back Electrostatic Field on Particle Fate

The next step was processing all particle trajectories using the VBA code to evaluate the final fate of the particles. In contrast to the conventional particulate control devices considering particle fate as either penetrated or collected, qualitative observations indicated a third category of "suspended", which is the fraction of incoming lunar dust unable to pass through the ELDC and not collected on the ELDC plate within the defined run time. On this basis, the particle fraction from each category (i.e., collected, penetrated or suspended) was plotted for different loadings of the pre-collected particles (see Fig. 5). For this particular ELDC dimension, the dust concentration ranged from 18 to 128 #/cm^3 to include the 50 #/cm^3 value reported by Surveyor-7 lander (Criswell, 1973). The upper limit for the number of the pre-collected particles was taken as 900 #/cm^2 in that collection efficiency dropped to zero at this particle loading even at the highest applied voltage.

In general, the ELDC collection efficiency starts dropping when the collection plate has accumulated a minimum number of particles. This threshold for collection efficiency depends on the applied voltage. While particles immediately started to be repelled for any number of pre-collected particles at ΔV = 50 V (see Fig. 5(a)), a relatively stronger e-field at ΔV = 100 V made the ELDC more resistive to the back e-field effect and no change in collection efficiency was detected for the number of pre-collected particles lower than 220 #/cm^2 (see Fig. 5(b)). However, as time went by and the number of collected particles increased, the back e-field gradually became stronger. Ultimately, the back e-field was so strong (> 900 #/cm^2) that no incoming lunar particles could be collected even at the higher voltage. Inferring from Figs. 5(a) and 5(b), back e-field enhancement led to significant deceleration in particle motion. Then, the majority of the particles that were not collected became suspended. Particle penetration continued for a while after attaining 0% collection efficiency (between 400 to 625 #/cm^2 at ΔV = 50 V, and between 625 to 900 #/cm^2 at ΔV = 100 V). Thereafter, similar to particle collection, particle penetration stopped.

Back e-field created by the build-up layer of already collected particles on the ELDC plate prevents incoming particles from both collection and penetration. In other words, the incoming particles are simultaneously under the influence of attraction forces from charges on ELDC plate, and the repelling forces from the like-charged previously collected particles and other approaching particles. This forms a cloud of particles in front of the protected surface deteriorating the performance of the ELDC and the pertinent device. Presumably, increasing the applied voltage postpones the final suspension (Figs. 5(b) vs. Fig. 5(a)).

The worst period of time in ELDC operation can be envisaged from two different perspectives. From surface protection point of view, the corresponding time for the highest possible particle penetration is when the ELDC becomes the least efficient. Although a decrease in particle penetration occurs thereafter, particle suspension strengthens at the same time which also lowers the performance of the protected surfaces, if the surface function is to receive solar radiation, e.g., solar panels.

It was also observed that for an ELDC with no pre-collected particles, the collection efficiency of the one with a higher incoming particle concentration was slightly lower. This confirms the results from our previous studies concluding that electrical particle-particle interactions, which increases when particle concentration increases, tend to make ELDC collection efficiency closer to 50% (Afshar-Mohajer *et al.*, 2012).

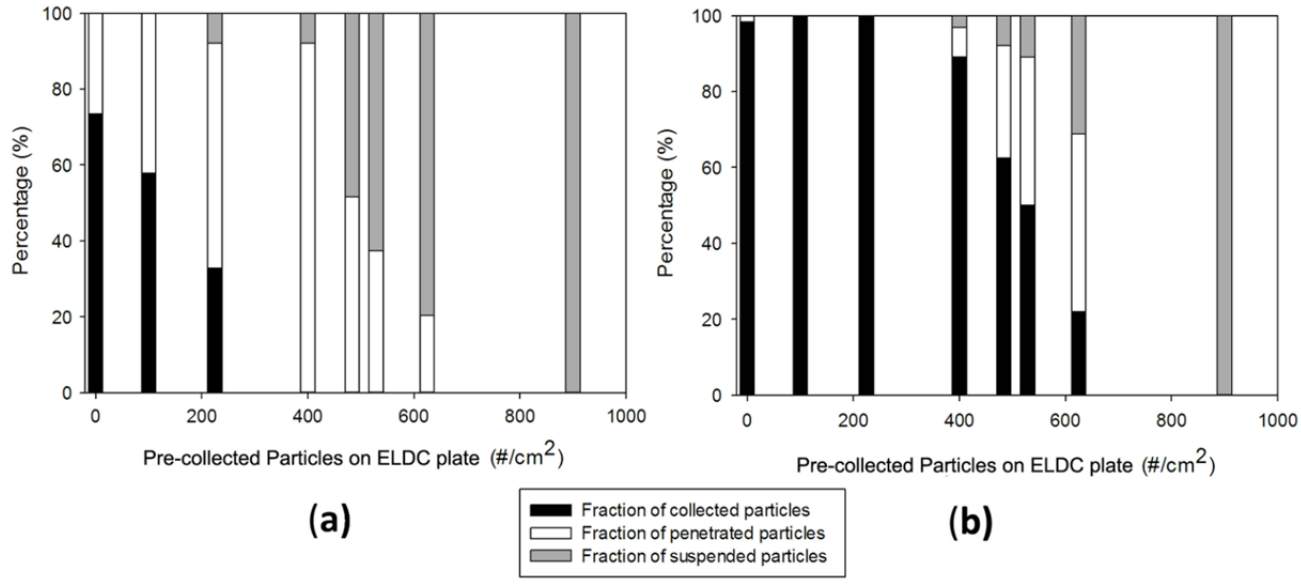

Fig. 5. Fate of incoming particles at 50 #/cm^3 by category and applied voltage: (a) ΔV = 50 V, and (b) ΔV = 100 V.

ELDC Collection Efficiency as a Function of Time

Estimating the frequency of the ELDC plate cleaning requires obtaining insight into how collection efficiency changes with time. Presenting a general analytical way to relate collection efficiency and elapsed time is very sophisticated as it involves many complicating factors. For example, two ELDCs with the same applied electrostatic field but different sizes may start with the same collection efficiency, but the larger ELDC has the capacity to hold more particles before the back e-field starts to affect the performance.

Nevertheless, an example is presented here to demonstrate how ELDC collection efficiency changes over time for given ELDC dimensions, operating conditions and particle characteristics. This requires the following simplifying assumptions:

- In order to maintain the particle number concentration constant, the following set of incoming particles enters the ELDC volume only after the elapsed time of the previous set of particles. This assumption is justified because the longest possible time for a particle to stay inside an ELDC with clean plates is quite short (0.08 s for 20-μm lunar dust to pass through 1 cm length of ELDC).
- Only an ELDC with > 90% collection efficiency is considered; in other words, cleaning is presumed when the collection efficiency drops below 90%.

Fig. 5(b) demonstrates that for any number of incoming particles, its collection efficiency at a particle loading of 400 #/cm^2 on the ELDC plates is higher than 90%. Thus, a final DEM simulation was run for the same ELDC sizing (L = W = 1 cm and D = 0.5 cm) with 25 (initially placed as in 5 rows and 5 columns) particles at ΔV = 100 V. Assuming the previously described time T = 0.16 s is adequate for either particle collection or penetration, the same number of incoming particles were fed from Particle Factory 2 after each 0.16 s to keep the particle concentration at 50 #/cm^3. The simulation run time was long enough to ensure 400 particles had been collected on the ELDC collection plates. Approximately, such a particle loading on ELDC collection plate occurred between the releases of the 19th and the 20th sets of incoming particles (see Fig. 6). The equivalent collection efficiency was 82.9% which is lower than the expected value of 90%. As shown in Fig. 5(b), suspension starts for particle loading greater than 200 #/cm^2; i.e., suspended particles accumulated from the earlier released sets caused such a reduction in collection efficiency.

However, this assumption of continuous lunar dust influx through the ELDC plates is very conservative. The deposition rate of the lunar particles on surfaces has not been measured meticulously during Apollo missions. The only relevant reported data has come from the studies on Surveyor 3 components after Apollo 12 mission. The lunar dust coverage on camera lens was roughly estimated as 25% of its surface area during 945 days of operation (0.8% per month) without human activities (Murphy *et al.*, 2010). Accordingly, the number of 20-μm-sized particles deposited presumably as a single layer on the surface is estimated to be 1273 #/month for the ELDC geometry used in this study. Thus, considering 400 #/cm^2 on the ELDC collection plate as the criterion for plate cleaning, the ELDC plates should be cleaned every 10 terrestrial day.

To clean the ELDC plates, the entire ELDC system can be detached from the protected surface. Then, switching the electrical polarities on the ELDC plates and shaking help dropping off the collected particles. Since the ELDC is basically an electrical capacitor collecting particles with negligible power consumption, applying such an electrical potential between the ELDC plates greater than the previously obtained values for 100% collection efficiency can reduce the frequency of plates cleaning even further.

ELDC Power Consumption

Assuming 10 × 10 cm plates with a 5 cm distance in between, 200 pairs of ELDC plates with 175 V applied

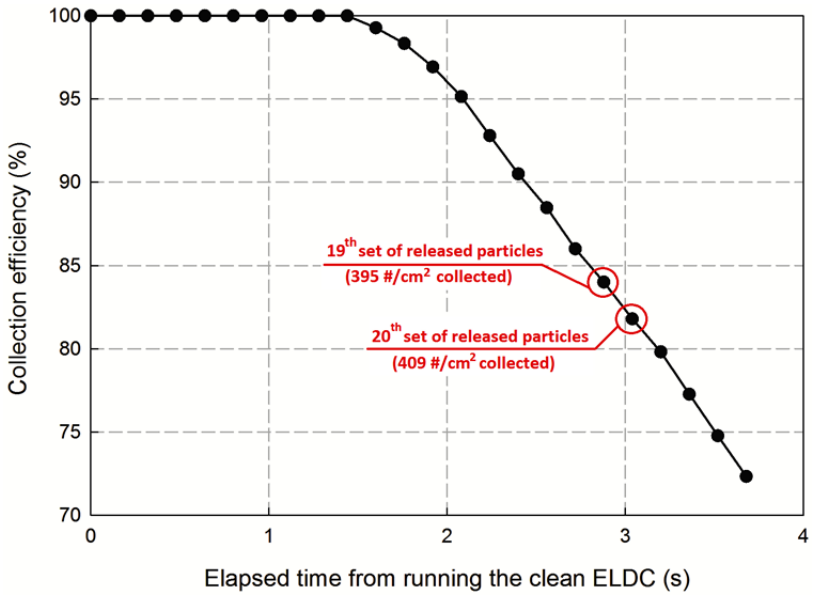

Fig. 6. Collection efficiency as a function of time for the described ELDC.

voltage between each pair of the plates are needed to cover 1 m^2 of the solar panel surface and to provide the previously obtained 3.5 kV/m electric field which runs a clean ELDC with 100% collection efficiency (Afshar-Mohajer *et al.*, 2012). Duke *et al.* (2001) estimated 65 W/m^2 as the provided electric power by a solar panel in lunar environment. Since the ELDC is practically a capacitor with vacuum as its insulator, the required power to run the ELDC can be approximated using the following the equation (Ulaby, 2010):

$$W = N \times \frac{1}{2}\frac{\varepsilon_0 A}{D}\Delta V^2 \quad (8)$$

where N is the number of plate pairs and A is the plate area (L × W). According to Eq. (8), 5.42×10^{-6} W/m^2 would be the required power for the ELDC described above, which is a negligible fraction of the produced 65 W/m^2 estimated by Duke *et al.* (2001). One should notice that ELDC only needs power supply connection initially to attain the maximum possible charges on its plate surfaces. Afterwards, ELDC becomes ideally a capacitor and the distributed charges would be maintained in the absence of the power supply.

CONCLUSIONS

In this study, the effect of back e-field due to particle build-up on the collection plates of an ELDC was investigated using a DEM model applicable for an ELDC of any size. The obtained results from tracking particle trajectories confirmed the formation of the circulation regions in proximity of the collection plate. The extracted plots from sensitivity analyses demonstrated that there were 3 stages in the operation of an ELDC. Initially, the clean ELDC was highly efficient in particle collection. The back e-field then enhanced gradually as more particles got collected; thus, a fraction of supposedly collected particles penetrated the ELDC due to repulsion from the collection plate. Eventually, the generated back e-field prevented all incoming particles from collection and penetration in a given time, due to counteraction with the ELDC electrostatic field. Such a suspension is undesirable in that it blocks light reaching the solar panel surface and it avoids any new incoming particles from collection.

Increasing the applied voltage from 50 V to 100 V enabled the ELDC to run with 100% collection efficiency at particle loadings less than 220 #/cm^2 whereas the ELDC operated under a lower voltage experienced an immediate reduction in collection efficiency. Increasing the number concentration of incoming particles decreased the rate of reduction in collection efficiency as it counteracted the effect of back e-field.

The last step of this study was relating the ELDC collection efficiency to the elapsed time of ELDC operation. While presenting a general explicit model for such a relationship is too sophisticated, the difference between an ELDC starting fresh and one with pre-collected dust was found. After collecting 400 #/cm^2 dust particles, the ELDC's collection efficiency was 83% compared to 90% of an ELDC with 400 #/cm^2 pre-collected particles. The suspended fraction was responsible for the difference. Using reported values from Surveyor 3 operation during Apollo 12, a rough estimation on how often the ELDC plate must be cleaned concluded 3 times per month as the required frequency for the plate cleaning. As the power consumption of the ELDC is just a negligible fraction of the power that can be produced by the solar panel (5.4×10^{-6} W/m^2 vs. 65 W/m^2), applying a cautiously higher electrical potential between the plates to alleviate back e-effect and therefore to reduce the frequency of plate cleaning is a viable option.

To more accurately determine the cleaning frequency of the ELDC, investigating the reduction rate of the produced electric power from a solar cell due to the dust deposition in vacuum environment is recommended. The electric power anticipated to be supplied by the solar cell determines the minimum ELDC collection efficiency needed at each time to replace the assumed 90% value of this study.

ACKNOWLEDGEMENT

We gratefully appreciate the financial support of the Space Research Initiative by the State of Florida (Grant No. 20040028). We are also thankful to DEM-Solutions Inc. for assistance in DEM modeling.

REFERENCES

Abbas, M., Tankosic, D., Craven, P., Spann, J., LeClair, A. and West, E. (2007). Lunar Dust Charging by Photoelectric Emissions. *Planet. Space Sci.* 55: 953–965.

Afshar-Mohajer, N., Damit, B., Wu, C.Y. and Sorloaica-Hickman, N. (2011). Electrostatic Particle Collection in Vacuum. *Adv. Space Res.* 48: 933–942.

Afshar-Mohajer, N., Damit, B., Wu, C.Y. and Sorloaica-Hickman, N. (2011). Efficiency Evaluation of an Electrostatic Lunar Dust Collector, 41st International Conference on Environmental Systems (ICES 2011), AIAA 2011-5201.

Afshar-Mohajer, N., Wu, C.Y. and Sorloaica-Hickman, N. (2012). Efficiency Determination of an Electrostatic Lunar Dust Collector by Discrete Element Method. *J. Appl. Phys.* 112: 023305-023305-023309.

Afshar-Mohajer, N., Wu, C.Y., Moore, R. and Sorloaica-Hickman, N. (2014). Design of an Electrostatic Lunar Dust Repeller for Mitigating Dust Deposition and Evaluation of its Removal Efficiency. *J. Aerosol Sci.* 69: 21–31.

Alshibli, K.A. and Hasan, A. (2009). Strength Properties of JSC-1A Lunar Regolith Simulant. *J. Geotech. Geoenviron. Eng.* 135: 673–679.

Calle, C., Buhler, C., Johansen, M., Hogue, M. and Snyder, S. (2011). Active Dust Control and Mitigation Technology for Lunar and Martian Exploration. *Acta Astronaut.* 69: 1082–1088.

Catalan-Izquierdo, S., Bueno-Barrachina, J.M., Cañas-Peñuelas, C.S. and Cavallé-Sesé, F. (2009). Capacitance Evaluation on Parallel-plate Capacitors by Means of Finite Element Analysis. Internation Conference on

Renewable Energies and Power Quality (ICREPQ).

Colwell, J.E., Robertson, S.R., Horányi, M., Wang, X., Poppe, A. and Wheeler, P. (2009). Lunar Dust Levitation. *J. Aerosp. Eng.* 22: 2–9.

Criswell, D. (1973). Horizon-glow and the Motion of Lunar Dust, In *Photon and Particle Interactions with Surfaces in Space,* Grard, R.J.L. (Ed.), 37: 545–556.

Cundall, P.A. and Strack, O.D.L. (1979). A Discrete Numerical Model for Granular Assemblies. *Geotechnique* 29: 47–65.

Di Renzo, A. and Di Maio, F.P. (2004). Comparison of Contact-Force Models for the Simulation of Collisions in DEM-Based Granular Flow Codes. *Chem. Eng. Sci.* 59: 525–541.

Dove, A., Dickson, S., Robertson, S., Sternovsky, Z., Wang, X. and Horányi, M. (2010). Characterization of a UV-Generated Photoelectron Sheath, 41st Lunar and Planetary Science Conference 41: 2406.

Duke, M.B., Ignatiev, A., Freundlich, A., Rosenberg, S.D. and Makel, D. (2001). Silicon PV Cell Production on the Moon as the Basis for a New Architecture for Space Exploration. *AIP Conference Proceedings* 552: 19.

Farrell, W., Stubbs, T., Vondrak, R., Delory, G. and Halekas, J. (2007). Complex Electric Fields near the Lunar Terminator: The Near-Surface Wake and Accelerated Dust. *Geophys. Res. Lett.* 34: 14.

Gaier, J.R. (2005). The Effects of Lunar Dust on EVA Systems during the Apollo Missions. NASA/TM, 213610, 2005.

Gaier, J.R., Waters, D.L., Misconin, R.M., Banks, B.A. and Crowder, M. (2011). Evaluation of Surface Modification as a Lunar Dust Mitigation Strategy for Thermal Control Surfaces, 41st International Conference on Environmental Systems (ICES 2011), AIAA 2011–5183.

Goertz, C. (1989). Dusty Plasmas in the Solar System. *Rev. Geophys.* 27: 271–292.

Halekas, J., Mitchell, D., Lin, R., Hood, L., Acuna, M. and Binder, A. (2002). Evidence for Negative Charging of the Lunar Surface in Shadow. *Geophys. Res. Lett.* 29: 77–71.

Halekas, J., Delory, G., Lin, R., Stubbs, T. and Farrell, W. (2008). Lunar Prospector Observations of the Electrostatic Potential of the Lunar Surface and its Response to Incident Currents. *J. Geophys. Res*. 113: A09102.

Hinds, W.C. (1982). *Aerosol Technology: Properties, Behavior, and Measurement of Airborne Particles*, 2nd Ed., Wiley-Interscience.

Liu, G., Marshall, J., Li, S. and Yao, Q. (2010). Discrete Element Method for Particle Capture by a Body in an Electrostatic Field. *Int. J. Numer. Methods Eng.* 84: 1589–1612.

Liu, Y., Park, J., Schnare, D., Hill, E. and Taylor, L.A. (2008). Characterization of Lunar Dust for Toxicological Studies. II: Texture and shape characteristics. *J. Aerosp. Eng.* 21: 272–279.

Manka, R.H. (1973). Plasma and Potential at the Lunar Surface, In *Photon and Particle Interactions with Surfaces in Space,* Grard, R.J.L. (Ed.), p. 347–361.

Mazumder, M., Biris, A., Sims, R., Calle, C. and Buhler, C. (2003). Solar Panel Obscuration in the Dusty Atmosphere of Mars, Proceedings ESA-IEEE Joint Meeting on Electrostatics p. 208–218.

Miller, J., Hoferer, B. and Schwab, A. (1998). The Impact of Corona Electrode Configuration on Electrostatic Precipitator Performance. *J. Electrostat.* 44: 67–75.

Mizuno, A. (2000). Electrostatic Precipitation. *IEEE Trans. Dielectr. Electr. Insul.* 7: 615–624.

Murphy T. Jr,, Adelberger, E., Battat, J., Hoyle, C., McMillan, R., Michelsen, E., Samad, R., Stubbs, C. and Swanson, H. (2010). Long-Term Degradation of Optical Devices on the Moon. *Icarus* 208: 31–35.

Nishiyama, H. and Nakamura, M. (1994). Form and Capacitance of Parallel-Plate Capacitors. *IEEE Trans. Compon. Packag. Manuf. Technol. Part A* 17: 477–484.

Park, J., Liu, Y., Kihm, K.D. and Taylor, L.A. (2008). Characterization of Lunar Dust for Toxicological Studies. I: Particle size distribution. *J. Aerosp. Eng.* 21: 266–271.

Qian, D., Marshall, J. and Frolik, J. (2011). Control Analysis for Solar Panel Dust Mitigation Using an Electric Curtain. *Renewable Energy* 41: 134–144.

Reitan, D.K. and Higgins, T.J. (1951). Calculation of the Electrical Capacitance of a Cube. *J. Appl. Phys.* 22: 223–226.

Reitan, D.K. (1959). Accurate Determination of the Capacitance of Rectangular Parallel-Plate Capacitors. *J. Appl. Phys.* 30: 172–176.

Schmitt, J., Heiken, G., Vaniman, D. and French, B.M. (1991). *Lunar Sourcebook: A User's Guide to the Moon*. Cambridge University Press.

Stubbs, T.J., Vondrak, R.R. and Farrell, W.M. (2006). A Dynamic Fountain Model for Lunar Dust. *Adv. Space Res.* 37: 59–66.

Tavarez, F.A. and Plesha, M.E. (2007). Discrete Element Method for Modelling Solid and Particulate Materials. *Int. J. Numer. Methods Eng.* 70: 379–404.

Ulaby, F.T. (2010). *Fundamentals of Applied Electromagnetics*, 6th Ed., Prentice Hall.

Walch, B., Horányi, M. and Robertson, S. (1995). Charging of Dust Grains in Plasma with Energetic Electrons. *Phys. Rev. Lett.* 75: 838–841.

Walton, O.R. (2007). Adhesion of Lunar Dust. NASA/CR-214685.

Wang, J., He, X. and Cao, Y. (2008). Modeling Electrostatic Levitation of Dust Particles on Lunar Surface. *IEEE Trans. Plasma Sci.* 36: 2459–2466.

Zukeran, A., Looy, P.C., Chakrabarti, A., Berezin, A.A., Jayaram, S., Cross, J.D., Ito, T. and Chang, J.S. (1999). Collection Efficiency of Ultrafine Particles by an Electrostatic Precipitator under DC and Pulse Operating Modes. *IEEE Trans. Ind. Appl.* 35: 1184–1191.

Received for review, December 13, 2013
Accepted, April 3, 2014